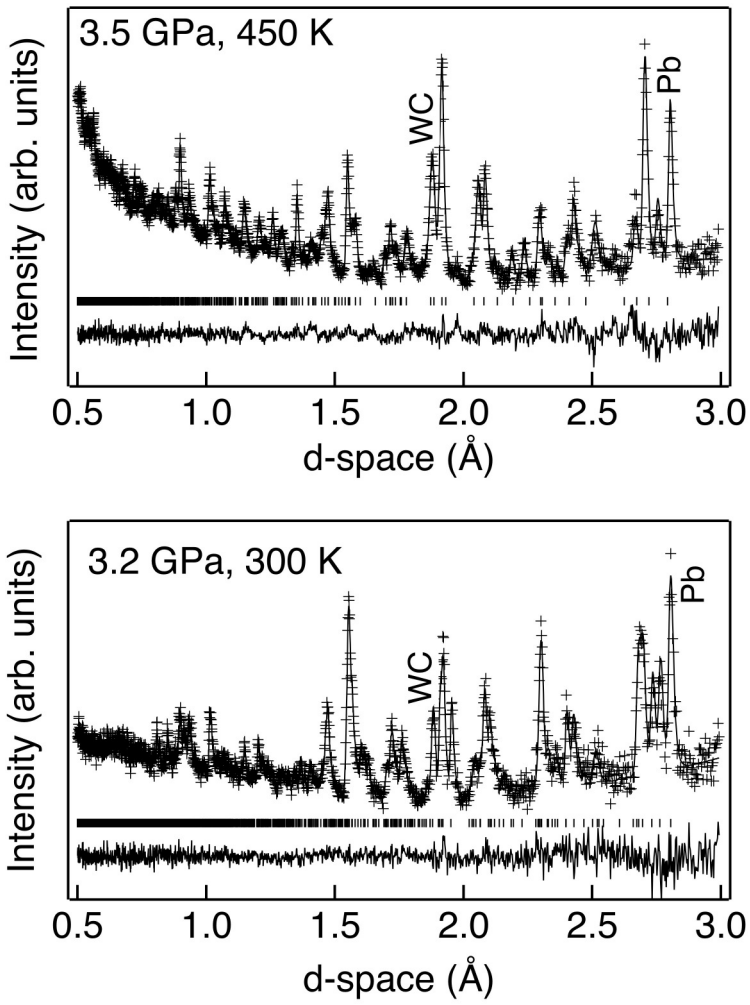

Supplementary Figure S1

Rietveld fits of the triclinic $BiNiO_3$ structure to ambient temperature data (300 K and 3.2 GPa) and the orthorhombic structure to high-temperature data (450 K and 3.5 GPa). Observed (points), calculated (full line) and difference profiles are shown together with Bragg markers for the $BiNiO_3$ phase. The peaks from WC and Pb are indicated.

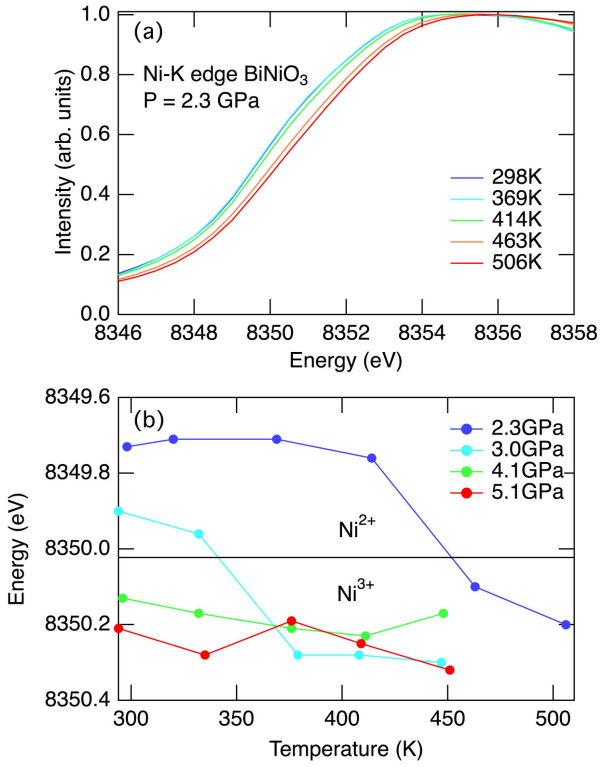

Supplementary Figure S2

(a) Ni-*K* edge XAS spectra for $BiNiO_3$ at various temperatures and 2.3 GPa. The edge energy E_0^K shifts to higher energy between 414 and 463 K indicating the Ni^{2+} to Ni^{3+} valence state change. This 0.5 eV shift is smaller than the value of 0.8 eV observed at room temperature probably because of the pressure dependence of the distribution between d^7 and $d^8\underline{L}$ electronic configurations in the Ni^{3+} state where $\underline{L}$ denotes a ligand (O 2*p*) hole as discussed in ref. 16. (b) Plots of E_0^K estimated at various pressures against temperature. The transition temperature is shifted down at 3 GPa and no temperature-induced transition was observed at 4.1 and 5.1 GPa. These results are consistent with our structural study.

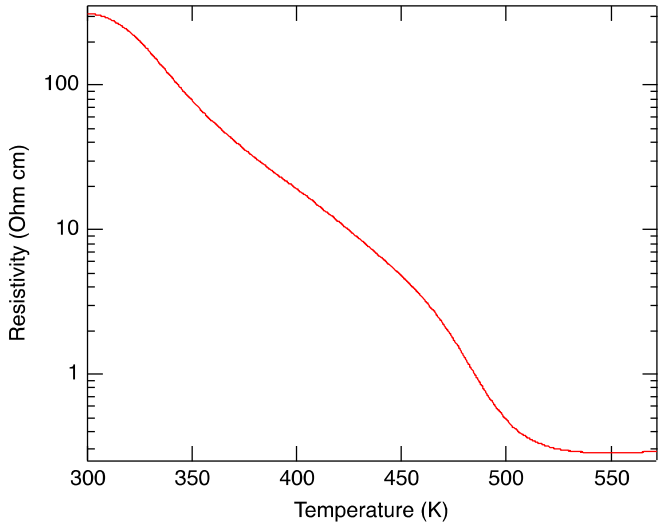

Supplementary Figure S3

The temperature dependence of the electrical resistivity of $BiNiO_3$ at 1.6 GPa showing an insulator-metal transition at around 530 K, consistent with the phase diagram in Fig. 3. The resistance was measured by a two-probe method with a cubic anvil type high-pressure apparatus.

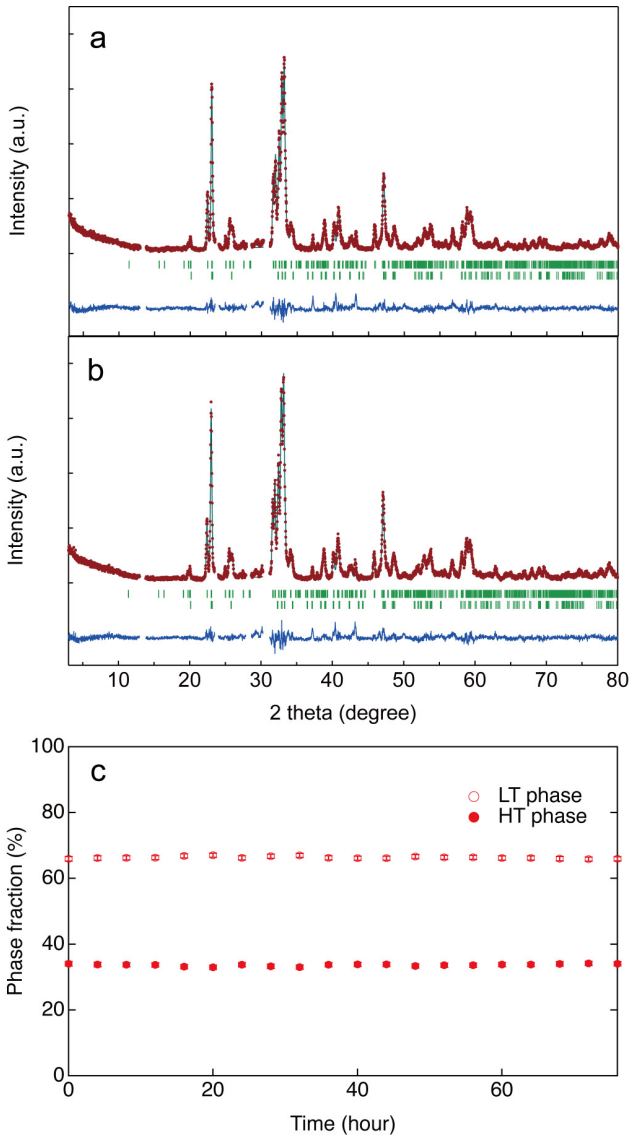

Supplementary Figure S4

Rietveld fits of the $Bi_{0.95}La_{0.05}NiO_3$ powder X-ray diffraction data collected immediately upon heating to 340 K in 10 K / min (a) and after holding at 76 h at this temperature (b). Observed (points), calculated (full line) and difference profiles are shown together with Bragg markers for the LT and the HT $BiNiO_3$ phases. (c) The fractions of the LT and the HT phases determined by Rietveld analysis, including error bars which are smaller than the points. reveal that the phase fractions do not alter.. The data were collected with Rigaku RINT-2500 diffractometer (Cu-kα radiation). About 3 mg of sample powder was pasted on a non-reflecting SiO_2 sample holder.

Supplementary Table S1. Crystallographic parameters for $BiNiO_3$ at 300 K/3.2 GPa and at 450 K/3.5GPa. The Bond Valence Sums calculated from the determined structural parameters are Bi1:3.46, Bi2:4.92, Ni1:1.83, Ni2:2.11, Ni3:2.04, Ni4:2.06 at 300 K / 3.2 GPa and are Bi:3.30, Ni:2.73 at 450 K / 3.5 GPa. These clearly show the change of the valence state from LPT $Bi^{3+}_{0.5}Bi^{5+}_{0.5}Ni^{2+}O_3$ to HPT $Bi^{3+}Ni^{3+}O_3$ revealing the temperature induced intermetallic charge transfer.

atom	site	x	y	z	$100 \times U_{iso}$ (Å^2)
300 K/3.2 GPa [a]					
Bi1	2i	0.0023(30)	0.0441(19)	0.2347(15)	0.43(17)
Bi2	2i	0.5107(29)	0.4411(21)	0.7238(16)	0.43(17)
Ni1	1d	0.5	0	0	0.22(8)
Ni2	1c	0	0.5	0	0.22(8)
Ni3	1f	0.5	0	0.5	0.22(8)
Ni4	1g	0	0.5	0.5	0.22(8)
O1	2i	0.8627(34)	0.4694(29)	0.2502(27)	0.09(9)
O2	2i	0.3935(35)	0.0780(29)	0.7539(22)	0.09(9)
O3	2i	0.8430(34)	0.1765(32)	-0.0306(23)	0.09(9)
O4	2i	0.3163(34)	0.3280(28)	0.0840(24)	0.09(9)
O5	2i	0.2149(34)	0.7666(34)	0.4138(24)	0.09(9)
O6	2i	0.6653(36)	0.6875(30)	0.5469(23)	0.09(9)
450 K/3.5 GPa [b]					
Bi1	4c	-0.0020(25)	0.0476(10)	0.25	0.50(14)
Ni1	4b	0.5	0	0	0.73(13)
O1	8d	0.6974(16)	0.2983(15)	0.0432(11)	1.20(18)
O2	4c	0.0884(19)	0.4710(19)	0.25	0.11(20)

[a] Space group *P*-1, $a = 5.3464(6)$ Å, $b = 5.6118(8)$ Å, $c = 7.6330(8)$ Å, $\alpha = 91.80(1)$ °, $\beta = 89.75(1)$ °, $\gamma = 90.954(9)$ °, $R_{WP} = 3.99$ %, $\chi^2 = 1.19$. The thermal parameters of Bi, Ni and O atoms are constrained.

[b] Space group *Pbnm*, $a = 5.3271(6)$ Å, $b = 5.5019(7)$ Å, $c = 7.6221(8)$ Å, $R_{WP} = 2.97$ %, $\chi^2 = 1.66$.